Sensors & Actuators: B. Chemical 331 (2021) 129350

Contents lists available at ScienceDirect

Sensors and Actuators: B. Chemical

journal homepage: www.elsevier.com/locate/snb

Silicon nanocrystals as signal transducers in ionophore-based fluorescent nanosensors

Mark S. Ferris [a,d,1], Ashley P. Chesney [a], Bradley J. Ryan [b], Utkarsh Ramesh [b], Matthew G. Panthani [b], Kevin J. Cash [a,c,*]

[a] Chemical and Biological Engineering Department, Colorado School of Mines, Golden, CO, 80401, United States
[b] Department of Chemical and Biological Engineering, Iowa State University, Ames, IA, 50011, United States
[c] Quantitative Biosciences and Engineering, Colorado School of Mines, Golden, CO, 80401, United States
[d] National Institute of Standards and Technology, Applied Physics Division, Physical Measurements Laboratory, 325 Broadway, Boulder, CO, 80305, United States

ARTICLE INFO

Keywords:
Silicon nanocrystals
Polymeric nanosensors
Biomedical sensors
Fluorescence

ABSTRACT

Colloidal silicon crystallites in the size range of 1−12 nm, also referred to as "silicon nanocrystals" have unique optical properties that include high quantum efficiency, size-dependent emission spanning the visible to near-infrared range, and robust photostability. These features, combined with silicon's high earth-abundance and good biocompatibility, make them an attractive option to serve as signal transduction elements in bioanalytical sensors. In this study, we combine silicon nanocrystals with a sodium-selective ionophore and a charge balancing additive in polymeric nanosensors to create a Silicon Nanocrystal NanoSensor (SiNC-NS). The SiNC-NS responded to sodium through a decrease in fluorescence intensity without the inclusion of a pH-sensitive absorbing dye which is normally included in analogous sensors for signal gating, leading to a sensor design with more photostable components. The SiNC-NS has a biologically relevant dynamic range of 4–277 mM Na^+, is selective against potentially interfering cations, and a reversible response between 0 and 2 M Na^+ for at least three cycles. This work shows the first sodium-responsive silicon nanocrystal-based sensor, the first use of silicon nanocrystals in polymeric nanosensors, and demonstrates an intriguing ionophore-mediated response in silicon nanocrystals to be explored further in the future.

1. Introduction

Silicon is one of the most abundant raw materials on earth, making it a low-cost and readily available material for industrial production, [1] and is the backbone of the microelectronics industry [1,2]. Bulk silicon is a poor light emitter due to its indirect bandgap; however, research over the last two decades has revealed that nanosized crystalline silicon, also referred to as silicon nanodots or silicon nanocrystals (SiNC), exhibits interesting structural and surface-dependent optical properties [1–3]. Like other semiconductor-based quantum dot compositions such as cadmium chalcogenides (Cd-chalcogenides), SiNCs have robust photostability [4] and high quantum yields [5], and their photon emission wavelength is tunable from the visible to infrared range by varying particle size [5]. However, unlike most semiconducting quantum dots that contain toxic metals such as Cd, SiNCs are understood to have good biocompatibility [6]. These unique optical features—combined with their cost advantage, resource-abundance, and biocompatibility—have led to interest in utilizing SiNCs in bioimaging and biosensing applications.

SiNCs as a technological platform are less-developed compared to their Cd-chalcogenide counterparts. Si-based nanomaterials are now attracting considerable attention for use as signal transducers in fluorescent sensors, [7–9] although the field is still in its early stages. Explosive materials such as nitrobenzene (NB), dinitrotoluene (DNT), and trinitrotoluene (TNT) have been shown to quench the luminescence of porous silicon through an electron transfer mechanism [10,11], leading to SiNC-based sensor platforms [12]. SiNCs have also shown sensitivities to toxic metal cations [13,14] neurotransmitters [15], and ethanol [16]. Enzyme-based detection strategies have been used to reach glucose [17] and pesticides as detectable analytes with SiNCs

Abbreviations: SiNC, Silicon Nanocrystal; SiNC-NS, Silicon Nanocrystal Nanosensor; R-, Additive; L, Ionophore.

* Corresponding author at: Chemical and Biological Engineering Department, Colorado School of Mines, Golden, CO, 80401, United States.
E-mail address: kcash@mines.edu (K.J. Cash).
[1] Current Address.

https://doi.org/10.1016/j.snb.2020.129350
Received 2 June 2020; Received in revised form 24 November 2020; Accepted 13 December 2020
Available online 25 December 2020

[18]. To reach analytes beyond those listed here with SiNC-based sensors, advanced sensing platforms are needed [20].

The application of SiNCs as a fluorescent signal transducer in polymeric nanosensors is currently unexplored in the literature. Polymeric nanosensors are an advanced type of sensor technology that have also attracted recent research attention for biomedical imaging and sensing [20,21]. In this work, we define polymeric nanosensors as any sensor that consists of a hydrophobic, plasticized-polymer core surrounded by an amphiphilic lipid-layer (for biocompatibility) [22–24], and where the necessary sensing chemicals are loaded into the plasticized polymer core. This allows for the use of different sensing schemes to reach a wide variety of analyte targets. Our lab utilizes poly(vinyl) chloride in the nanosensor core and our sensors have an average size ranging from ~140 nm to ~200 nm, though other groups make similar sensors with different polymers [21]. The polymeric nanosensor platform is versatile and allows for non-invasive detection with three-dimensional spatial resolution. Their fluorescent readouts also allow for continuous and remote monitoring. This set of attributes makes polymeric nanosensors ideal for advanced bio-monitoring applications where other sensor classes fall short [25].

For ion sensing, polymeric nanosensors commonly use an ionophore-based detection mechanism. This consists of an ion-binding molecule ("ionophore") for analyte recognition coupled to a pH-responsive fluorescent molecule for signal transduction through maintaining a charge-balance in the organic phase. However, the organic fluorophores that are typically used for signal transduction in these schemes often have poor photostability and high interference from biological entities. Static fluorophores such as quantum dots, [26,27] carbon dots [23], and persistent luminescent strontium aluminate particles [28] can also be utilized with a slight variation on this mechanism whereby these elements are paired with a non-fluorescent pH-sensitive absorbing dye for signal gating.

In this work, we present the first use of SiNCs for signal transduction in ionophore-based polymeric nanosensors, and the first report of a Na^+-selective SiNC-based sensor in a platform that we term Silicon Nano-Crystal NanoSensor (SiNC-NS). While Na^+-selective sensors are analyzed in this report, we present a generalizable, nanosized platform where SiNCs can be used to analyze a range of ion targets. We achieved a selective response to Na^+ over potentially competing ions without the use of a non-fluorescent pH-sensitive dye for signal gating by utilizing SiNCs coupled with a Na^+-binding ionophore in polymeric nanosensors, a process which is depicted in Fig. 1. We also characterize the sensor in terms of response time, dynamic range, reversibility, and stability.

2. Materials and methods

2.1. Reagents and materials

Poly(vinyl chloride) (PVC), high molecular weight PVC, bis(2-ethylhexyl) sebacate (BEHS), tetrahydrofuran (THF), dichloromethane (DCM), Sodium tetrakis[3,5-bis(trifluoromethyl)phenyl]borate, Selectophore (NaBARF), 4-(2-hydroxyethyl)pipera- zine-1- ethanesulfonic acid (HEPES), 4-tert-Butylcalix arene-tetraacetic acid tetraethyl ester (sodium ionophore X (NaI X); Selectophore™), sodium chloride (NaCl), potassium chloride (KCl), lithium chloride (LiCl), calcium chloride ($CaCl_2$), and silicon monoxide (SiO, 325 mesh) were purchased from Sigma Aldrich (St. Louis, MO). 1,2-Disteroyl-sn-glycero-3-phosphoethanolamine-N- [methoxy(polyethylene glycol)-750] ammonium salt in chloroform (PEG-lipid) was purchased from Avanti Polar Lipids (Alabaster, AL). Hydrochloric acid concentrate (HCl; 10 N, ACS certified), sodium hydroxide concentrate (NaOH; 10 N, ACS certified), and 2-Amino-2-hydroxymethylpropane-1,3-diol, 2 M solution (TRIS, 2 M) were purchased from Fisher Scientific (Waltham, MA). Hydrofluoric acid (HF, aqueous, 48 %) was purchased from Acros Organics (Geel, Belgium). 1-dodecene (96 %) was purchased from Alfa Aesar (Haverhill, MA). Phosphate buffered saline (PBS, pH = 7.4) was purchased from Life Technologies (Grand Island, NY).

2.2. Silicon nanocrystal synthesis

The SiNCs were synthesized by modifying a procedure reported by Sun et al. [29]. Briefly, 4.2 g of silicon monoxide was placed in an alumina boat and transferred into a tube furnace. The furnace was then purged with forming gas (5 mol % H_2, 95 mol % N_2) for 2 h and subsequently heated from room temperature to 300 °C at 14 °C/min, and held at 300 °C for 20 min. Then, the furnace was heated to 600 °C at 14 °C/min and held at 600 °C for 20 min. Finally, the furnace was heated to 910 °C at 14 °C/min and held at 910 °C for 1 h before turning off the furnace and allowing the furnace to cool naturally to room temperature. The entirety of the heating process was performed under a forming gas flow of ~1 mL/min. This heating process yields silicon nanocrystals embedded in an amorphous silicon oxide matrix. Once cooled to room

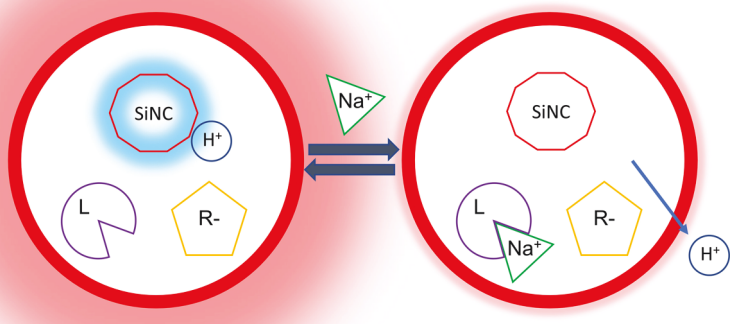

Fig. 1. Scheme depicting sensor components, including silicon nanocrystals (SiNCs), Na^+ binding ionophore (L), and charge balancing additive (R-). As the concentration of Na^+ ions increases in the sample, Na^+ binds to the ionophore (L), inducing a decrease in fluorescence from the SiNC. Na^+ binding to the additive also causes positive charges (such as H^+) to migrate out of the nanosensor core to maintain charge neutrality.

temperature, the oxide-embedded SiNCs were ground to a fine powder with a mortar and pestle, and then transferred to a flask containing glass beads, and shaken with a wrist-action shaker overnight.

To liberate the SiNCs from the oxide matrix, 2.4 *g* of the powder was etched in the dark for 4 h with a mixture of 33 mL HF (48 %) and 4.4 mL HCl (32 %). *Caution! HF is extremely dangerous and should only be handled by extensively-trained personnel.* After etching, the mixture was centrifuged at 11,000 rpm for 10 min, the supernatant was discarded, and the precipitates were washed twice with ethanol and once with chloroform with centrifugation and decantation after each solvent addition; each washing step used 60 mL of respective solvent and was centrifuged at 11,000 rpm for 10 min.

After washing, the SiNCs were then immediately transferred to a round-bottomed three-neck flask with 13 mL of 1-dodecene and subject to three freeze-pump-thaw cycles on a Schlenk line under flowing N_2. The SiNCs were then heated to 190 °C overnight. After the reaction, the SiNCs were cooled to room temperature and washed three times by precipitating with methanol, centrifuging at 9000 rpm for 5 min, decanting the supernatant, and dissolving in toluene. After the last decantation, the SiNCs were dissolved in toluene, filtered through a 0.45 μm PTFE filter, and subsequently dried under vacuum and kept under nitrogen for characterization.

2.3. SiNC-NS formulation

SiNC-NS were fabricated similar to previously established method for ion-selective nanosensors, [30] though with slight variations. Briefly, an optode cocktail was formulated by dissolving 15 mg PVC and 33 μL BEHS (1:2 by mass) along with 1.5 mg NaIX and 0.5 mg NaIX in THF. 4.4 mg of SiNCs were then dissolved in DCM. 2 mg PEG-lipid (80 μL of a 25 mg/mL solution in chloroform) was dried and resuspended in 5 mL HEPES/TRIS buffer (pH = 7.4) with a probe tip sonicator for 30 s at 20 % intensity (Branson, Danbury CT). Then, 50 μL of optode cocktail solution and 50 μL of SiNC/DCM solution were mixed before immediately injecting into the PBS/PEG-lipid solution while under probe tip sonication (3 min, 20 % intensity). The resultant nanosensor solution was filtered with a 0.8 μm syringe filter to remove excess polymer (Pall Corporation, Port Washington, NY).

2.4. Procedures

2.4.1. Silicon nanocrystal characterization

Powder X-ray Diffraction: XRD data were collected with a Bruker D8 Advance diffractometer with a Cu Kα radiation source. Data were collected by placing a dry powder of the SiNCs in an acrylic substrate.

UV–vis Absorbance: Absorbance data were collected on a PerkinElmer Lambda 750 spectrophotometer. The nanocrystals were dissolved in chloroform for UV–vis data acquisition.

Steady State Photoluminescence: PL data were collected on an Ocean Optics JAZ spectrometer. The excitation source was a 405 nm LED. The nanocrystals were dissolved in chloroform for PL data acquisition.

Fourier Transform Infrared Spectroscopy: FTIR data were collected with a Nicolet iS5 FTIR spectrometer with an iD5 attenuated total reflectance (ATR) accessory.

Transmission Electron Microscopy: TEM images were recorded using an FEI Tecnai G2-F20 instrument operated at 200 kV. The nanocrystals were dissolved in chloroform and deposited onto a 200 mesh copper grid coated with amorphous carbon.

2.4.2. SiNC-NS analysis

2.4.2.1. Response time, selectivity, and dose/response analysis. Analyte solutions were prepared at double the test concentration in HEPES/TRIS solution (buffered at pH = 7.4). 100 μL of nanosensors and 100 μL of analyte solution were mixed in each well of a column in a 96 well plate to obtain the desired analyte concentration. One well in each row contained 0.1 N HCl and one contained 0.1 N NaOH (to determine the maximum and minimum signal in polymeric nanosensors). A Synergy H1 microplate reader (BioTek, Winooski, Vermont, USA) was used to collect photoluminescence intensity with an excitation of 390 nm and an emission of 700 nm. Data was collected in triplicate for each experiment except for reversibility testing. Data was collected immediately after mixing SiNS-NCs with analyte solution and then every minute for 1 h.

The SiNC-NS response was determined using a similar approach to prior work [23]. Briefly, the data was normalized between 10^{-6} M Na and fully deprotonated (0.1 N NaOH), and fit to a four parameter logistic response curve, with the key metric being the $LogEC_{50}$ which is the concentration corresponding to half-maximal response. The response range was then defined by the x-axis range when a tangent line at $LogEC_{50}$ deviates less than 5% from the non-linear fit to Na^+ response. The SiNC-NS selectivity was determined by the Nicolskii-Eisenman model for a fixed interfering ion [31,32]. The SiNC-NS response time was determined by first fitting the midpoint of the dynamic range of the Na^+ response over time to a two-phase decay equation,

$$Y = Plateau + SpanFast * e^{(-kFast*X)} + SpanSlow * e^{(-kSlow*X)}$$

$$SpanFast = (Y0 - Plateau) * \%Fast * .01$$

$$SpanSlow = (Y0 - Plateau) * (100 - \%Fast) * .01$$

where Y0 is the initial sensor $LogEC_{50}$, Plateau is the final sensor $LogEC_{50}$, kFast and kSlow are the rate constants of the fast and slow phases in units that are the reciprocal of the X axis units, and %Fast is the percent of the Y signal due to the fast phase. The response time was then determined to be the time for the curve to decay 90 % from the Y0 value to the Plateau value.

2.4.2.2. pH response. To test the sensor response to pH, a large batch of SiNC-NS were concentrated via centrifugal filtration, aliquoted into 8 portions, and resuspended in HEPES/TRIS solutions adjusted to different pH levels before fluorescence testing in the manner described above (2.4.2.1 Response time, selectivity, and dose/response analysis).

2.4.2.3. Reversibility. Reversibility testing followed a previously established procedure [23]. SiNC-NS were concentrated via ultrafiltration (Amicon Ultra – 0.5 mL, 30 K NMWL, Merck Millipore Ltd, Tullagreen, Carrigtwohill, Co. Cork, IRL) and sealed in 13 kDa MWCO hollow fiber dialysis tubing (Spectra/Por® In Vivo, Spectrum Laboratories Inc., Rancho Dominquez, CA, USA) on the bottom of a 6-well plate (Sterile, untreated 6-well microplate, flat bottom, w/ lid, polystyrene, Caplugs Evergreen, Buffalo, NY, USA) using underwater epoxy (WaterWeld™ Epoxy Putty, J-B Weld, Atlanta, GA, USA). The sealed SiNC-NS were conditioned in 2 mL HEPES/TRIS (pH = 7.4) for 3 h before initial measurements. After initial measurements, the test solutions were alternated between either 2 M Na^+ and HEPES/TRIS or between 0.1 N HCl and 0.1 N NaOH, washing 3x with Millipore H_2O in between each solution change and measuring the sensor signal after 1 h in each solution. The sensor signal was measured with the Synergy H1 used above by first recording photoluminescence intensity over an 11 × 5 area scan with a 1600μM × 1600μM spacing and with a 360 nm excitation and 700 nm emission collection. Raw intensity values across from the brightest 5% of pixels in the area scan were then averaged to determine the sensor signal with standard deviation used as error bars.

2.4.2.4. Stability. For stability measurements, SiNC-NS fluorescence dose/response to Na^+ was monitored over 14 days (testing occurred on days 1, 2, 3, 7, and 14. Several batches of SiNC-NS were prepared in the manner described above (section 2.3 SiNC-NS formulation) and combined. The SiNC-NS were stored in the dark at room temperature when

not undergoing testing in the manner described above (section 2.4.2.1). A Welch's *t*-test was applied to test for a significant decrease in the $LogEC_{50}$ from one test day to the next.

3. Results and discussion

3.1. SiNC synthesis and characterization

Powder X-ray diffraction of the oxide-embedded SiNCs (Fig. 2a) indicate phase-pure SiNCs, with a broad feature at ~21.5° 2Theta corresponding to the amorphous silicon oxide matrix. Scherrer analysis on the peaks corresponding to the (220) and (311) planes indicate nanocrystal sizes of 3.7 and 4.1 nm, respectively. Note that the (111) peak was omitted from this analysis due to the overlap with the amorphous feature. FTIR of the dodecene-terminated SiNCs is shown in Fig. 2b. The SiNCs show characteristic CH_X stretching modes at 2958, 2918, 2849 cm^{-1}, and bending modes at 1458, 1412, 1376 cm^{-1}. Residual SiH_X (where x = 1, 2, or 3) stretching modes from the etching procedure are present with a peak at 2083 cm^{-1}. The Si-C bonds corresponding to SiNC passivation have vibrational frequencies at 1258, 793, and 662 cm^{-1}. Silicon oxide species related to incomplete etching and processing the SiNCs in air are present as stretching modes at 1086, 1012, and 793 cm^{-1}.

The optical properties of the dodecene-terminated SiNCs were characterized using UV–vis absorbance and steady-state photoluminescence (Fig. 2c). The absorbance spectrum shows a nearly featureless curve, with a shoulder at ~325 nm (~3.8 eV) that corresponds to the direct Γ → Γ transition [33,34]. The steady-state photoluminescence is centered at 810 nm with a FWHM of 220 nm, corresponding to 0.47 eV. According to the effective mass approximation (EMA)—which is known to underestimate nanocrystal diameters [5,35]—a PL peak position of 810 nm implies a SiNC diameter of ~2.9 nm, which agrees well with the aforementioned XRD Scherrer analysis. Further, TEM of SiNCs (Fig. 2d) also demonstrate nanocrystals with diameters on the order of 5 nm. These structural and vibrational characterizations demonstrate that we have successfully synthesized phase-pure silicon nanocrystals that are terminated with dodecene, with residual Si-H and SiO bonds. These residual bonds may play a role in the SiNC-NS mechanism discussed below. Additionally, the optical characterization of the isolated nanocrystals provide a baseline for SiNC-NS characterization.

3.2. SiNC-NS development and characterization

Silicon Nanocrystal Nanosensors (SiNC-NS) were created by combining SiNCs with an ionophore (for analyte recognition and selectivity), an additive (for charge balance control), and a polymer, plasticizer, and surfactant for the nanosensor structure. Use of a static lumophore with an ionophore-based mechanism in polymeric nanosensors normally requires a non-fluorescent pH-sensitive dye for signal gating, [23,26,28] but we found the SiNC-NS to be responsive to Na^+ without this component (Fig. 3). This indicates that the SiNCs are participating in the sensor mechanism rather than remaining inert, potentially through a pH mediated response similar to other nanosensors. Fig. 3a shows the normalized fluorescence of the SiNC-NS recorded initially after addition of analyte solutions and then every five minutes for 60 min total (all intensity data normalized between intensity at 10^{-6} M Na^+ and intensity at 0.1 N NaOH). The SiNC-NS increased their raw fluorescence over time in response to 0.1 N HCl and decreased their fluorescence in response to a range of Na^+ solutions and 0.1 N NaOH (See Fig. S1 for raw dose/response curves). Fig. 3b shows the midpoint of the dynamic range of the SiNC-NS ($LogEC_{50}$) over

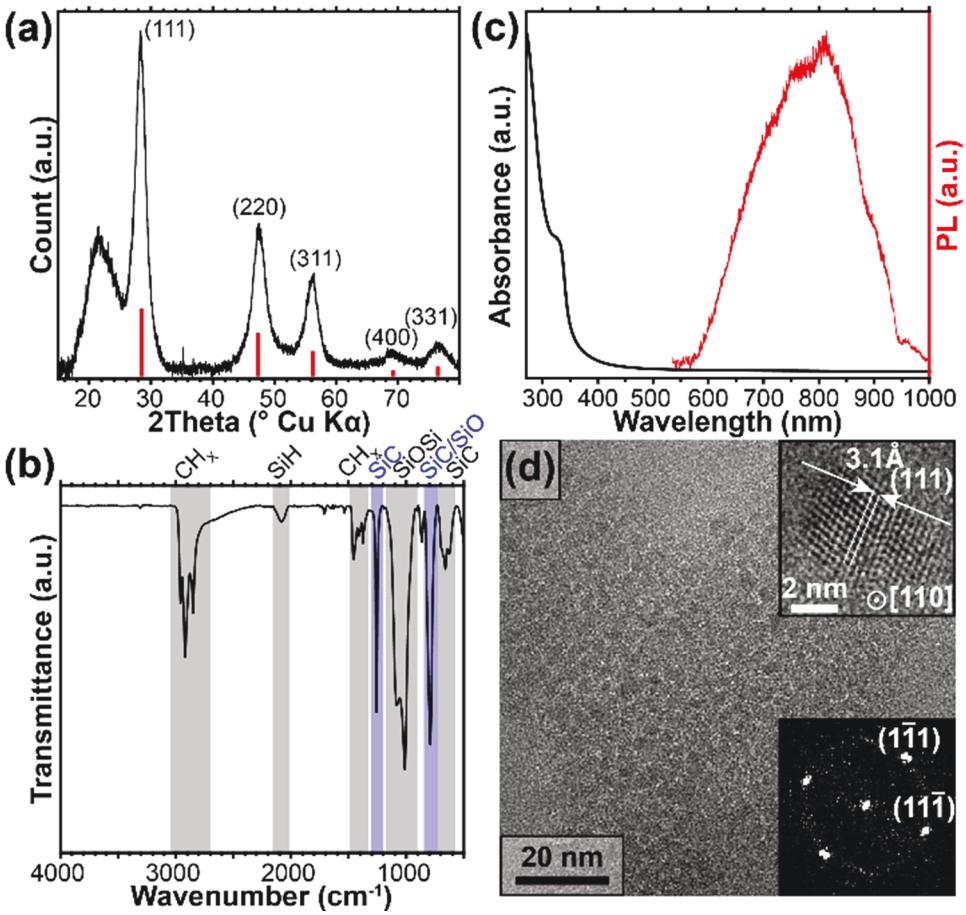

Fig. 2. Structural, optical, and chemical characterization of the SiNCs. (a) Powder X-ray diffraction of oxide-embedded SiNCs. The red stick pattern corresponds to bulk silicon. (b) FTIR of dodecene-terminated SiNCs; blue labels are to help with peak differentiation. (c) UV–vis absorbance (black, left axis) and steady-state photoluminescence (red, right axis) of dodecene-terminated SiNCs in chloroform. (d) TEM of dodecene-terminated SiNCs; the top right inset is an HRTEM image and the bottom right inset is the FFT of the top right inset.

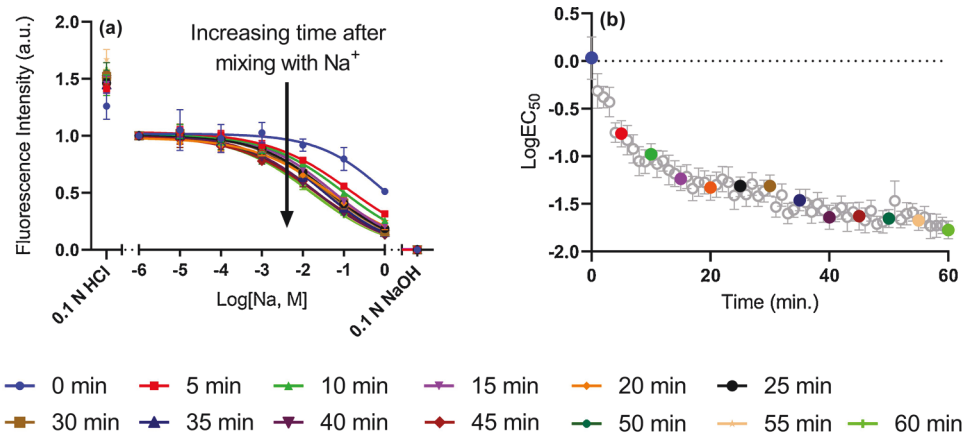

Fig. 3. Response time of SiNC-NS. (a) Dose/response curves showing the response of SiNC-NS to 0.1 N HCl, a range of Na^+ concentrations, and 0.1 N NaOH immediately after the initial addition (blue circles, top curve) and every five minutes thereafter (n = 3, error bars show the standard deviation for three technical replicates). (b) Progression of the midpoint of the response curve ($LogEC_{50}$) over time after analyte addition, yielding a T_{90} of 77 min. Where error bars are not shown, the error bars are smaller than the data point.

time after analyte addition with a time resolution of one minute. While ionophore-based nanosensors normally respond instantaneously to analyte solutions due to their thermodynamic equilibrium-based response mechanism [32,36] and fast kinetic steps due to their small size [37], SiNC-NS responded to Na^+ with a "fast" component and a "slow" component on a time scale of roughly one hour (T_{90} = 77 min, Fig. 3b). This slower response time further indicates a slower kinetic step in the response for the SiNC-NS than comparable ionophore-based nanosensors in this class. To account for the response time, in all subsequent data analysis the sensor response was measured one hour after combining with analyte solutions.

The dynamic range and selectivity of the SiNC-NS were analyzed by measuring the sensor response to Na^+ and potentially interfering cations over a wide concentration range. The sensors have a dynamic range of 4 mM–277 mM (Fig. 4a), bracketing the physiologic range expected in blood (135–145 mM). The response midpoint is 52 mM ($LogEC_{50}$ of -1.28), which aligns with our recent report of an ionophore-mediated sodium sensor [28]. The sensors have selectivity coefficients of -1.6, -2.2 over the potentially interfering cations K^+ and Li^+, similar to other sensor devices made with the same ionophore [26,28,38]. A nonlinear regression of the Ca^{2+} response failed to converge due to the minimal response at higher Ca^{2+} concentrations. As a control experiment, the Na^+-selective ionophore was removed from the sensor formulation and the responses to Na^+ and K^+ were measured. As expected with removal of the selective agent, the sensors are no longer selective for Na^+ over K^+, as shown in Fig. 4b. This indicates that the SiNCs do not have a direct response to the sample Na^+ concentration and that the sensor mechanism and selectivity are mediated by the ionophore.

To probe a potentially pH-mediated response mechanism further, we tested the fluorescence intensity of the SiNC-NS when exposed to varying pH. Fig. 5a shows the raw fluorescence of the SiNC-NS in different pH solutions. In addition to a large immediate response to changes in pH, there was also a slower response to intermediate pH values (8–11). The fluorescence of the SiNC-NS one hour after addition of pH solutions was plotted against pH in Fig. 5b, showing the SiNC-NS to be responsive to pH over a wide range. Importantly, this pH is the solution pH rather than the effective pH inside the organic phase of the nanoparticle, which is drastically different from the external solution pH [39]. Similar to organic chromoionophores, the pK_a of a proton responsive moiety (e.g. chromoionophore or SiNC) in a membrane can be orders of magnitude away from solution pH, but due to the proton exchange equilibrium the effective pK_a of the nanosensor encapsulated group can be shifted [39]. The clear responsiveness to pH when encapsulated inside nanosensors indicates that the SiNCs may function similar to the chromoionophores used in typical ionophore-based formulations rather than static fluorophores such as carbon dots [23] or upconversion luminescence dyes [40]. The "fast" and "slow" nature of the SiNC-NS response to pH notably also is seen in the SiNC-NS response to Na^+ (Fig. 3a), indicating that the sensor mechanism is likely pH-mediated in addition to being ionophore-mediated, as described above.

Fig. 6 shows the reversibility of the SiNC-NS between HEPES/TRIS buffer (pH = 7.4) and 2 M Na^+ while Fig. S2 shows the reversibility of the SiNC-NS between 0.1 N HCl and 0.1 N NaOH. SiNC-NS were sealed in a microdialysis tube with 13 kDa cutoff and adhered to the bottom of a well so that when analyte solutions are flowed over the sample, the solutions can be exchanged while SiNC-NS are retained within the tube [23,24]. As expected, SiNC-NS consistently lose and recover their fluorescence between exposure to HEPES/TRIS and 2 M Na^+. This indicates that the SiNC interaction with Na^+ is reversible. The variability of the sensor signal between different cycles of HEPES/TRIS is likely due to sensor migration within the microdialysis tube, which we commonly observe when using this method for nanosensor reversibility testing [23,

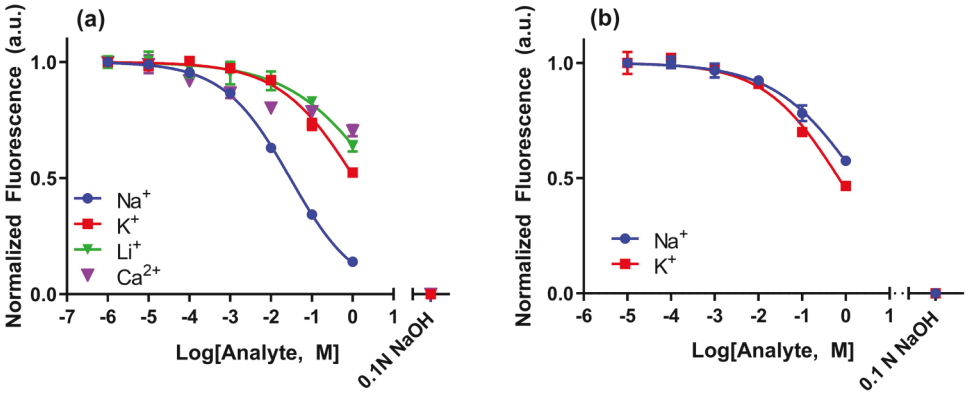

Fig. 4. (a) Dose-response curves of SiNC-NS showing the selectivity for Na^+ over the potentially interfering cations K^+, Li^+, and Ca^{2+} (n = 3, error bars show the standard deviation of three technical replicates). (b) SiNC-NS lose their selectivity for Na^+ over K^+ when sodium ionophore is removed from the formulation (n = 3, error bars show the standard deviation of three technical replicates) indicating that the response of the sensors is ionophore mediated. Where error bars are not shown, the error bars are smaller than the data point.

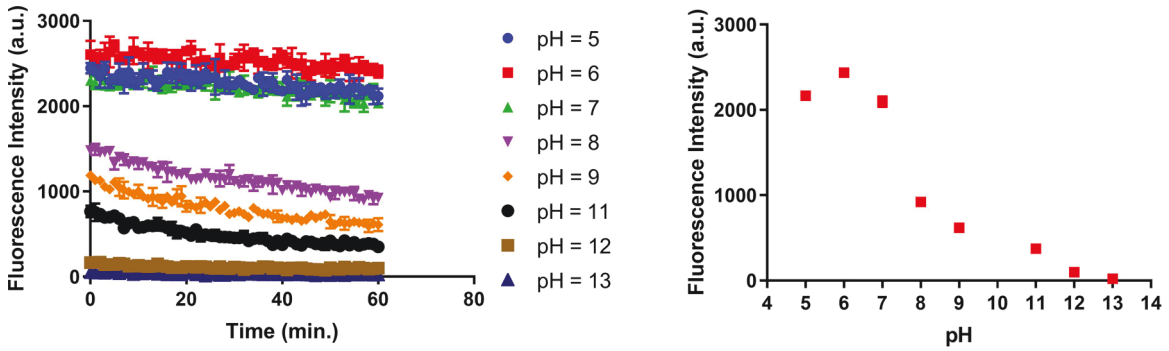

Fig. 5. (a) SiNC-NS response to pH over time (n = 3, error bars show the standard deviation of technical replicates). (b) SiNC-NS dose/response curve to pH, one hour after addition of pH solutions. This indicates that the sensor mechanism is impacted by pH of the sample solution as expected from a pH mediated mechanism. Where error bars are not shown, the error bars are smaller than the data point.

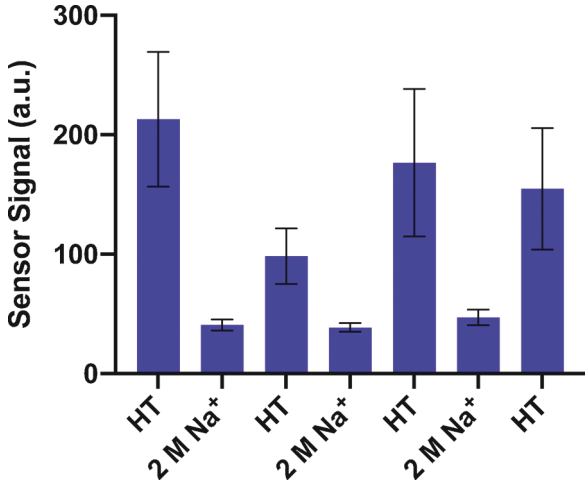

Fig. 6. Reversibility of the SiNC-NS fluorescence signal between 0 M and 2 M Na^+. The sensors were alternated between a HEPES/TRIS solution and 2 M Na^+ for three cycles and were able to recover fluorescence after being exposed to Na^+ during each cycle. Error bars represent standard deviation of pixel intensity.

40]. Notably, there is no overall diminishing trend between cycles of HEPES/TRIS, indicating that the process is reversible and that no permanent change is affecting the SiNC. However, when cycling between strong acid and base conditions (0.1 N HCl and 0.1 N NaOH, Fig. S2), the sensors gradually lost their ability to recover fluorescence in the 0.1 N HCl condition. This indicates that the nanosensor-encapsulated SiNCs are not protected to reaction with NaOH (e.g. $Si + 4NaOH \longrightarrow Na_4SiO_4 + 2H_2$) [41].

Finally, we examined the long-term stability of the SiNC-NS, as shown in Fig. 7. The SiNC-NS response to Na^+ changed in two ways over time. First, the response slowly shifts towards higher concentrations. A Welch's *t*-test concluded that a significant decrease in the $LogEC_{50}$ occurred between days 1 and 2, days 3 and 7, and days 7 and 14. The shift of the response towards higher concentrations over time moves the dose/response curve from the baseline normalized response (Fig. 7a) to that of the ionophore free control (Fig. 3b), and is indicative of ionophore slowly leaching from the sensor core. However, in analogous organic dye-based sensors, the response is typically stable over 1–2 weeks, [23] and swapping organic fluorophores for SiNC is unlikely to cause ionophore leaching. However, loss of ionophore fits with the trend seen in the data and should be investigated more in future experiments. The second change is a variability in absolute fluorescence intensity at low Na^+ concentrations (Fig. S3), indicating a change in the baseline fluorescence of the silicon nanocrystals. While they are stable in typical solvents [42], this is potentially an artifact of their inclusion in the environment inside the nanosensors. Also, during nanosensor synthesis, the SiNCs are dissolved in tetrahydrofuran which is known to passivate their fluorescence. The recovery in fluorescence seen over time is potentially a recovery from this passivation, since tetrahydrofuran is expected to evaporate later during synthesis. While it seems unlikely that changes in the SiNC are responsible for the shift in SiNC-NS response toward higher concentration described above, little is known about SiNC stability in the plasticized polymer environment and should be investigated in future experiments.

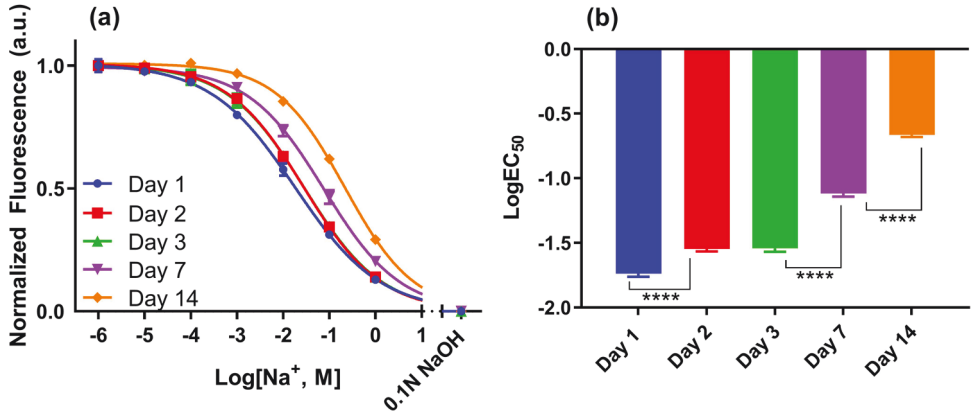

Fig. 7. Stability Testing. (a) Normalized fluorescence dose/response curves for the SiNC-NS over 14 days. (b) Drift of the SiNC-NS $LogEC_{50}$ over 14 days. **** represents a significant difference in $LogEC_{50}$ with $p < 0.0001$.

3.3. Discussion

The SiNC-NS presented here is comparable to other ionophore-mediated fluorescence sensors in the literature for most analytical features. Swapping SiNC for standard organic fluorophores has no effect on the size or biocompatibility of the sensor. The dynamic range of the sensor, 4 mM–277 mM, is similar to other recent ionophore-mediated Na^+ sensor reports [28] and covers the physiologically relevant range of Na^+ (135–145 mM). The selectivity of the SiNC-NS is also in line with most reports, [26,28,38] though there are now some strategies that lead to notably improved selectivity [43]. The SiNC-NS also shows satisfactory reversibility in normal operating conditions, though extreme pH environments irreversibly affects SiNCs. The SiNC-NS is notably slow compared to other sensors in its class, and improvement will be the focus of future work. The strength of the SiNC-NS compared to others in the class comes from the unique and optimal features of the SiNC. SiNC have high photostability and brightness comparable to carbon dots and quantum dots, without the toxicity issues of quantum dots. The SiNC-NS platform also does not require a pH-sensitive absorbing dye, unlike similar sensors that use carbon dots, quantum dots, or phosphorescent microparticles, improving the overall photostability of the system. In addition, SiNC have size-controllable emission in the visible to near-IR range, a powerful tool that can be used to create application-optimized sensors through both minimized background interference and minimized overlap with ratiometric dyes. For more comparisons of the analytical response between this work and other sodium sensors, see Table S1 in the supplementary material.

The data presented in this paper allows us to develop an informed theory on the sensor response mechanism. It is clear from the data presented in Fig. 4 that the mechanism is ionophore mediated. It is also clear from Fig. 7 that the SiNC-NS is responsive to pH. The evidence suggests that the SiNC-NS may be responding to a pH change in the nanosensor core triggered by the event of Na^+ extraction by the ionophore into the nanosensor core, similar to the way that ionophore-based optical sensors operate when organic fluorophores are used for signal transduction. However, unlike with organic fluorophores, in both the response to Na^+ shown in Fig. 3a and the response to pH in Fig. 7, there appear to be “fast” and “slow” components. It is well-understood that luminescence-quenching defects are introduced to SiNCs by removing hydrogen atoms from the surfaces; in aqueous environments, studies have shown a loss of hydrogen termination and concomitant reduction in photoluminescence in alkaline aqueous environments [44–46]. This change in photoluminescence intensity is reversible, and can be regained by passivating the surface with hydrogen, which is known to happen to SiNCs in acidic aqueous environments [44]. The “fast” and “slow” responses may be due to the fact that alkyl-terminated SiNC surface sites are only partially occupied by alkyl groups, and also contains Si-H, $Si-H_2$, and SiH_3 groups [47] that may possess different reaction kinetics. For example, some sites may be more easily accessed, such corner or edge sites on a faceted SiNC; whereas Si-H sites are expected to primarily lie on planar facets that may be sterically hindered by alkyl groups attached to proximal surface atoms. We cannot exclude the possibility that certain $Si-H_X$ sites are more reactive than others, nor is there evidence to support this. Given current understanding of the chemistry of the SiNC surface, we propose that (in alkaline environments) the patchy alkyl-terminated SiNC surfaces have some $Si-H_X$ sites that are more readily accessible and quickly dehydrogenated (causing the “fast” response), and other sites Si that dehydrogenate slower, most likely due to steric protection from the dodecyl groups. We should note that this mechanism depends on assumptions regarding the pH experienced by the SiNC; however, the true pH within the nanosensor is unknown. The mechanism that we propose here is consistent with the current understanding of the complex surface chemistry of SiNCs and their pH dependent-emission, and accounts for the pH-dependence of the SiNC-NS both with and without the ionophore; however, more experiments are necessary to confirm this mechanism and will be the focus of future experiments.

The current shortcomings of the SiNC-NS documented above, such as the fast and slow response, degradation in response to strong acid/base solutions, and limited shelf-life are not necessary inherent flaws in the platform, and have the potential to be addressed in future studies. For example, SiNC are known to be exceptionally bright, but their total emission is passivated substantially in the SiNC-NS formulation due to the use of tetrahydrofuran (data not shown) as a solvent for PVC and BEHS during nanosensor synthesis. The next-generation of SiNC-NS should aim to reformulate the particles by replacing tetrahydrofuran with toluene and a compatible polymer/plasticizer combination to substantially increase the brightness of the sensor. Future work should also focus on improving upon the combined fast and slow response kinetics of the SiNC-NS. If diffusion-limited surface reactions are responsible for the sluggish behavior (as we propose), then improvements could be brought about by engineering of the SiNC surface. For example, using shorter alkyl-chain surface ligands that pose a lower steric barrier, or ligands that are otherwise designed to make the surface more readily accessible may offer faster response times. In addition, the response time may be improved by incorporating surface functionalization techniques that have previously demonstrated to increase the pH-sensitivity of SiNC photoluminescence [19].

4. Conclusions

In this work, we developed and characterized a silicon nanocrystal nanosensor (SiNC-NS) for Na^+ detection by replacing the standard organic chromoionophore reporter with fluorescent silicon nanocrystals in a typical ionophore-based optical sensor formulation. The SiNC-NS responded to Na^+ without the inclusion of a non-fluorescent pH-sensitive dye for signal gating, though the Na^+-selective ionophore was shown to be necessary to impart selectivity to Na^+ over competing ions. This work therefore shows the first use of SiNCs for signal transduction in polymeric nanosensors and the first report of an ionophore-mediated fluorescence response from SiNCs. The nanosensors were able to detect changes in Na^+ concentration over the typical physiologic range, with a response midpoint of 52 mM, and a reversible response. With additional development, these SiNC-based nanosensors show promise to be a photostable alternative to organic fluorophores for and offer the benefit of fine-tunable emission wavelength for cation-responsive polymeric nanosensors

Funding sources

This research was supported with startup funds provided by Colorado School of Mines and the Colorado School of Mines Chemical and Biological Engineering Department. M.G.P acknowledges partial support from the National Science Foundation Early CAREER Development Award (Award # DMR-1,847,370), the Air Force Office of Scientific Research (AFOSR; Grant No. FA9550-20-1-0018), and the Herbert L. Stiles Faculty Fellowship from Iowa State University. B.J.R. acknowledges support from the National Science Foundation Graduate Research Fellowship Program under DGE 1744592. Any opinions, findings, and conclusions or recommendations expressed in this material are those of the authors and do not necessarily reflect the views of the National Science Foundation.

CRediT authorship contribution statement

Mark S. Ferris: Methodology, Validation, Formal analysis, Investigation, Data curation, Writing - original draft, Writing - review & editing, Visualization. **Ashley P. Chesney:** Validation, Investigation. **Bradley J. Ryan:** Visualization, Formal analysis, Investigation, Writing - review & editing. **Utkarsh Ramesh:** Investigation, Writing - review & editing. **Matthew G. Panthani:**Conceptualization, Methodology, Supervision, Funding acquisition, Writing - review & editing. **Kevin J.**

Cash: Conceptualization, Resources, Supervision, Supervision, Project administration, Funding acquisition, Writing - review & editing.

Declaration of Competing Interest

The authors declare no competing financial interest.

Appendix A. Supplementary data

Supplementary material related to this article can be found, in the online version, at doi:https://doi.org/10.1016/j.snb.2020.129350.

References

[1] B. Song, Y. He, Fluorescent silicon nanomaterials: from synthesis to functionalization and application, Nano Today 26 (2019) 149–163.
[2] L. Canham, Gaining light from silicon, Nature 408 (2000) 411–412.
[3] B.J. Ryan, M.P. Hanrahan, Y.J. Wang, U. Ramesh, C.K.A. Nyamekye, R.D. Nelson, et al., Silicene, Siloxene, or silicane? Revealing the structure and optical properties of silicon nanosheets derived from calcium disilicide, Chem. Mater. 32 (2020) 795–804.
[4] Y.L. Zhong, B. Song, F. Peng, Y.Y. Wu, S.C. Wu, Y.Y. Su, et al., In situ rapid growth of fluorescent silicon nanoparticles at room temperature and under atmospheric pressure, Chem. Commun. 52 (2016) 13444–13447.
[5] C.M. Hessel, D. Reid, M.G. Panthani, M.R. Rasch, B.W. Goodfellow, J.W. Wei, et al., Synthesis of ligand-stabilized silicon nanocrystals with size-dependent photoluminescence spanning visible to near-infrared wavelengths, Chem. Mater. 24 (2012) 393–401.
[6] S. Bhattacharjee, I. Rietjens, M.P. Singh, T.M. Atkins, T.K. Purkait, Z.J. Xu, et al., Cytotoxicity of surface-functionalized silicon and germanium nanoparticles: the dominant role of surface charges, Nanoscale 5 (2013) 4870–4883.
[7] C.M. Gonzalez, J.G.C. Veinot, Silicon nanocrystals for the development of sensing platforms, J. Mater. Chem. C Mater. Opt. Electron. Devices 4 (2016) 4836–4846.
[8] X.Y. Ji, H.Y. Wang, B. Song, B.B. Chu, Y. He, Silicon nanomaterials for biosensing and bioimaging analysis, Front. Chem. 6 (2018) 9.
[9] H.Y. Wang, Y. He, Recent advances in Silicon nanomaterial-based fluorescent sensors, Sensors 17 (2017) 15.
[10] S. Content, W.C. Trogler, M.J. Sailor, Detection of nitrobenzene, DNT, and TNT vapors by quenching of porous silicon photoluminescence, Chem. Eur. J. 6 (2000) 2205–2213.
[11] I.N. Germanenko, S.T. Li, M.S. El-Shall, Decay dynamics and quenching of photoluminescence from silicon nanocrystals by aromatic nitro compounds, J. Phys. Chem. B 105 (2001) 59–66.
[12] A. Nguyen, C.M. Gonzalez, R. Sinelnikov, W. Newman, S. Sun, R. Lockwood, et al., Detection of nitroaromatics in the solid, solution, and vapor phases using silicon quantum dot sensors, Nanotechnology 27 (2016) 12.
[13] J. Zhang, S.H. Yu, Highly photoluminescent silicon nanocrystals for rapid, label-free and recyclable detection of mercuric ions, Nanoscale 6 (2014) 4096–4101.
[14] B. Liao, W. Wang, X.T. Deng, B.Q. He, W.N. Zeng, Z.L. Tang, et al., A facile one-step synthesis of fluorescent silicon quantum dots and their application for detecting Cu2+, RSC Adv. 6 (2016) 14465–14467.
[15] X.D. Zhang, X.K. Chen, S.Q. Kai, H.Y. Wang, J.J. Yang, F.G. Wu, et al., Highly sensitive and selective detection of dopamine using one-pot synthesized highly photoluminescent silicon nanoparticles, Anal. Chem. 87 (2015) 3360–3365.
[16] Z.H. Zhang, R. Lockwood, J.G.C. Veinot, A. Meldrum, Detection of ethanol and water vapor with silicon quantum dots coupled to an optical fiber, Sensors and Actuators B-Chemical 181 (2013) 523–528.
[17] Y.M. Shen, X.Y. Zhang, X. Huang, Y.Y. Zhang, C.X. Zhang, J.L. Jin, et al., A new fluorescence and colorimetric sensor for highly selective and sensitive detection of glucose in 100% water, RSC Adv. 5 (2015) 63226–63232.
[18] Y.H. Yi, G.B. Zhu, C. Liu, Y. Huang, Y.Y. Zhang, H.T. Li, et al., A label-free silicon quantum dots-based photoluminescence sensor for ultrasensitive detection of pesticides, Anal. Chem. 85 (2013) 11464–11470.
[19] Y.L. Feng, Y.F. Liu, C. Su, X.H. Ji, Z.K. He, New fluorescent pH sensor based on label-free silicon nanodots, Sensors and Actuators B-Chemical 203 (2014) 795–801.
[20] G. Rong, S.R. Corrie, H.A. Clark, In vivo biosensing: progress and perspectives, ACS Sens. 2 (2017) 327–338.
[21] X.J. Xie, E. Bakker, Ion selective optodes: from the bulk to the nanoscale, Anal. Bioanal. Chem. 407 (2015) 3899–3910.
[22] M.S. Ferris, A.G. Katageri, G.M. Gohring, K.J. Cash, A dual-indicator strategy for controlling the response of ionophore-based optical nanosensors, Sens. Actuators B Chem. 256 (2018) 674–681.
[23] A.A. Galyean, M.R. Behr, K.J. Cash, Ionophore-based optical nanosensors incorporating hydrophobic carbon dots and a pH-sensitive quencher dye for sodium detection, Analyst 143 (2018) 458–465.
[24] M.P. Jewell, A.A. Galyean, J. Kirk Harris, E.T. Zemanick, K.J. Cash, Luminescent nanosensors for ratiometric monitoring of three-dimensional oxygen gradients in laboratory and clinical *Pseudomonas aeruginosa* biofilms, Appl. Environ. Microbiol. 85 (2019) e01116–19.
[25] J.M. Dubach, S. Das, A. Rosenzweig, H.A. Clark, Visualizing sodium dynamics in isolated cardiomyocytes using fluorescent nanosensors, Proc Natl Acad Sci 106 (2009) 16145–16150.
[26] J.M. Dubach, D.I. Harjes, H.A. Clark, Ion-selective nano-optodes incorporating quantum dots, J. Am. Chem. Soc. 129 (2007) 8418–8419.
[27] A. Sahari, T.T. Ruckh, R. Hutchings, H.A. Clark, Development of an optical nanosensor incorporating a pH-Sensitive quencher dye for potassium imaging, Anal. Chem. 87 (2015), 10684–7.
[28] M.S. Ferris, M.R. Behr, K.J. Cash, An ionophore-based persistent luminescent 'Glow Sensor' for sodium detection, RSC Adv. 9 (2019) 32821–32825.
[29] W. Sun, C.X. Qian, X.S. Cui, L.W. Wang, M.A. Wei, G. Casillas, et al., Silicon monoxide - a convenient precursor for large scale synthesis of near infrared emitting monodisperse silicon nanocrystals, Nanoscale 8 (2016) 3678–3684.
[30] J.M. Dubach, M.K. Balaconis, H.A. Clark, Fluorescent nanoparticles for the measurement of ion concentration in biological systems, J. Vis. Exp. (2011) 1–5.
[31] E. Bakker, W. Simon, Selectivity of ion-sensitive bulk optodes, Anal. Chem. 64 (1992) 1805–1812.
[32] K. Seiler, W. Simon, Theoretical aspects of bulk optode membranes, Analytical Chimica Acta 266 (1992) 73–87.
[33] B.G. Lee, J.W. Luo, N.R. Neale, M.C. Beard, D. Hiller, M. Zacharias, et al., Quasi-direct optical transitions in Silicon Nanocrystals with intensity exceeding the bulk, Nano Lett. 16 (2016) 1583–1589.
[34] J.D. Holmes, K.J. Ziegler, R.C. Doty, L.E. Pell, K.P. Johnston, B.A. Korgel, Highly luminescent silicon nanocrystals with discrete optical transitions, J. Am. Chem. Soc. 123 (2001) 3743–3748.
[35] P.F. Trwoga, A.J. Kenyon, C.W. Pitt, Modeling the contribution of quantum confinement to luminescence from silicon nanoclusters, J. Appl. Phys. 83 (1998) 3789–3794.
[36] G. Mistlberger, G.A. Crespo, E. Bakker, Ionophore-based optical sensors, in: R. G. Cooks, J.E. Pemberton (Eds.), Annual Review of Analytical Chemistry, Vol 7, Annual Reviews, Palo Alto, 2014, pp. 483–512.
[37] J.M. Dubach, D.I. Harjes, H.A. Clark, Fluorescent ion-selective nanosensors for intracellular analysis with improved lifetime and size, Nano Lett. 7 (2007) 1827–1831.
[38] J.M. Dubach, N. Zhang, E. Lim, K.P. Francis, H.A. Clark, *In Vivo* Sodium Concentration Continuously Monitored with Fluorescent Sensors, Integr. Biol. (Camb) 3 (2011) 142–148.
[39] Y. Qin, E. Bakker, Quantitive bindin constants of H+ -selective chromoionophores and anion ionophores in solvent polymeric sensing membranes, Talanta 58 (2002) 909–918.
[40] M.P. Jewell, M.D. Greer, A.L. Dailey, K.J. Cash, Triplet-Triplet annihilation upconversion based nanosensors for fluorescence detection of potassium, ACS Sens. (2020).
[41] F. Erogbogbo, T. Lin, P.M. Tucciarone, K.M. LaJoie, L. Lai, G.D. Patki, et al., On-demand hydrogen generation using nanosilicon: splitting water without light, heat, or electricity, Nano Lett. 13 (2013) 451–456.
[42] B.F.P. McVey, R.D. Tilley, Solution Synthesis, Optical Properties, and Bioimaging Applications of Silicon Nanocrystals, Acc. Chem. Res. 47 (2014) 3045–3051.
[43] R.J. Wang, X.F. Du, Y.T. Wu, J.Y. Zhai, X.J. Xie, Graphene quantum dots integrated in lonophore-based fluorescent nanosensors for Na+ and K+, ACS Sens. 3 (2018) 2408–2414.
[44] M. Cannas, P. Camarda, L. Vaccaro, F. Amato, F. Messina, T. Fiore, et al., Enhancing the luminescence efficiency of silicon-nanocrystals by interaction with H+ ions, J. Chem. Soc. Faraday Trans. 20 (2018) 10445–10449.
[45] K.K. Chen, K. Liao, G. Casillas, Y. Li, G.A. Ozin, Cationic silicon nanocrystals with colloidal stability, pH-Independent positive surface charge and size tunable photoluminescence in the near-infrared to red spectral range, Adv. Sci. 3 (2016), 1500263.
[46] A. Benilov, I. Gavrilchenko, I. Benilova, V. Skryshevsky, M. Cabrera, Influence of pH solution on photoluminescence of porous silicon, Sens. Actuators A Phys. 137 (2007) 345–349.
[47] M.P. Hanrahan, E.L. Fought, T.L. Windus, L.M. Wheeler, N.C. Anderson, N. R. Neale, et al., Characterization of silicon nanocrystal surfaces by multidimensional solid-state NMR spectroscopy, Chem. Mater. 29 (2017) 10339–10351.

M. S. Ferris received a Ph.D. in Chemical Engineering at Colorado School of Mines in 2019. Currently he is completing a National Research Council Postdoctoral Research Associateship at the National Institute of Standards and Technology in Boulder, CO, where his research focus is developing MRI-compatible sensor devices.

A. P. Chesney is pursuing a B.S. in Chemical Engineering in the Chemical and Biological Engineering Department at Colorado School of Mines, with an expected graduation date in 2022. Her research focus is development of optical nanosensors for biological monitoring.

B. J. Ryan received his B.S. in Chemical Engineering at Iowa State University. He is currently pursuing his Ph.D. in Chemical Engineering also at Iowa State University, where his research focuses on the characterization of two-dimensional silicon nanomaterials for optoelectronic applications.

U. Ramesh received his B.S. in Chemical Engineering at the University of Illinois at Urbana-Champaign. He is currently pursuing his master's in chemical engineering at Iowa State University, where his research focuses on the synthesis and characterization of two-dimensional Group IV nanomaterials.

M. G. Panthani is an Assistant Professor and Herbert L. Stiles Faculty Fellow in the Department of Chemical and Biological Engineering at Iowa State University. He earned a Ph.D. in Chemical Engineering from the University of Texas at Austin in 2011, and a B.S. in Chemical Engineering from Case Western Reserve University in 2006. He started as an Assistant Professor at Iowa State University in 2014, after completing a postdoctoral appointment in the Department of Chemistry at University of Chicago. His research focuses on inorganic materials chemistry related to electronic and optoelectronic technologies.

K. J. Cash received his Ph.D. in Chemical Engineering at the University of California Santa Barbara. He is currently an Assistant Professor in the Chemical and Biological Engineering Department at Colorado School of Mines. His lab's research is focused on the development, optimization, and application of fluorescent nanosensors for biological monitoring.